JGR Atmospheres

RESEARCH ARTICLE
10.1029/2020JD033339

Special Section:
The Exceptional Arctic Polar Vortex in 2019/2020: Causes and Consequences

Simulation of Record Arctic Stratospheric Ozone Depletion in 2020

Jens-Uwe Grooß[1] and **Rolf Müller**[1]

[1]Institute of Energy and Climate Research – Stratosphere (IEK-7), Forschungszentrum Jülich, Jülich, Germany

Abstract In the Arctic winter/spring of 2019/2020, stratospheric temperatures were exceptionally low until early April and the polar vortex was very stable. As a consequence, significant chemical ozone depletion occurred in the Arctic polar vortex in spring 2020. Here, we present simulations using the Chemical Lagrangian Model of the Stratosphere that address the development of chlorine compounds and ozone in the Arctic stratosphere in 2020. The simulation reproduces relevant observations of ozone and chlorine compounds, as shown by comparisons with data from the Microwave Limb Sounder, Atmospheric Chemistry Experiment-Fourier Transform Spectrometer, balloon-borne ozone sondes, and the Ozone Monitoring Instrument. Although the concentration of chlorine and bromine compounds in the polar stratosphere has decreased by more than 10% compared to peak values around the year 2000, the meteorological conditions in winter/spring 2019/2020 caused unprecedented ozone depletion. The lowest simulated ozone mixing ratio was about 40 ppbv. Because extremely low ozone mixing ratios were reached in the lower polar stratosphere, chlorine deactivation into HCl occurred as is normally observed in the Antarctic polar vortex. The depletion in partial column ozone in the lower stratosphere (potential temperature from 350 to 600 K, corresponding to about 12–24 km) in the vortex core was calculated to reach 143 Dobson Units, which is more than the ozone loss in 2011 and 2016, the years which —until 2020— had seen the largest Arctic ozone depletion on record.

Plain Language Summary In Arctic winter and spring 2019/2020, the stratospheric temperatures were exceptionally low for a long time period. This caused an unprecedented Arctic ozone depletion. We show simulations that represent this ozone depletion. The simulated ozone mixing ratios compare well with satellite and in situ observations.

Key Points:

- The Arctic vortex was exceptionally cold and stable in winter 2019/2020 resulting in substantial Arctic ozone depletion
- Arctic ozone loss in 2020 exceeded that in the cold Arctic springs of 2011 and 2016 that had previously shown the strongest ozone depletion
- Significant chlorine deactivation into HCl occurred, as is regularly observed in Antarctica

Supporting Information:

Supporting Information may be found in the online version of this article.

Correspondence to:
J.-U. Grooß,
j.-u.grooss@fz-juelich.de

Citation:
Grooß, J.-U., & Müller, R. (2021). Simulation of record Arctic stratospheric ozone depletion in 2020. *Journal of Geophysical Research: Atmospheres*, *126*, e2020JD033339. https://doi.org/10.1029/2020JD033339

Received 19 JUN 2020
Accepted 2 JUN 2021

1. Introduction

It is well established that the Antarctic ozone hole (Farman et al., 1985; Jones & Shanklin, 1995) is caused by chemical ozone depletion in austral spring through catalytic cycles driven by chlorine and bromine compounds (e.g., Solomon, 1999; WMO, 2018). For these cycles to run efficiently, chlorine needs to be activated from the reservoir compounds HCl and $ClONO_2$ by heterogeneous reactions. These heterogeneous reactions only take place at low temperatures typically present in polar winter and spring, occurring on the surfaces of Polar Stratospheric Clouds (PSCs) and on cold sulfate aerosol (e.g., Drdla & Müller, 2012; Portmann et al., 1996; Solomon, 1999; Tritscher et al., 2021; WMO, 2018).

Enhanced stratospheric halogen loading, commonly referred to as Equivalent Effective Stratospheric Chlorine (EESC), is caused by chlorine and bromine released from anthropogenically emitted chlorofluorocarbons (CFCs) and halons (Engel et al., 2018; Newman et al., 2007). Due to the regulations of the Montreal Protocol, including its amendments and adjustments, stratospheric halogen loading peaked around the year 2000. Due to the long atmospheric lifetime of the CFCs and halons, the EESC (polar winter conditions) was in 2020 only about 11%–12% lower than its peak value in 2002 (Engel et al., 2018; Newman et al., 2007; WMO, 2018). This level roughly corresponds to the EESC of 1992. In addition to the long-term decline of EESC in the atmosphere, there is also an inter-annual variability of inorganic chlorine (Cl_y, i.e., the sum of the destruction products of anthropogenically emitted CFCs) in the polar stratosphere, which is caused by the inter-annual variability of descent in the polar vortex (Strahan et al., 2014). In Antarctica, the expected decline of Cl_y is about −20 pptv/y, whereas the year-to-year variability ranges from −200 pptv to +150 pptv (Strahan et al., 2014). This effect is also present in the Arctic and underlines the importance of an accurate representation of diabatic descent for a given year in studies of polar ozone loss.

Due to the greater dynamical activity in the Arctic, which results in a less stable and warmer polar vortex, Arctic ozone depletion is typically much less pronounced and much more variable than in the Antarctic (e.g., Solomon, 1999; WMO, 2018). Stratospheric temperatures in the Arctic in winter and spring are generally much higher than those in the Antarctic, where low temperatures are the key factor in the formation of the ozone hole. However, strong chemical ozone loss has been identified in cold Arctic polar winters and springs exhibiting a persistent polar vortex into spring, for example in March 1997, 2011, and 2016 (Douglass & Kawa, 1999; Johansson et al., 2019; Kuttippurath et al., 2012; Manney & Lawrence, 2016; Manney et al., 2011; Müller et al., 1997; Newman et al., 1997; Sinnhuber et al., 2011; Tilmes et al., 2004; Weber et al., 2011; WMO, 2018). For Arctic ozone loss to occur, a stable vortex is required as well as temperatures below a threshold of about 195 K to trigger chlorine activation. These conditions exhibit large inter-annual variation. Low temperatures do not need to cover the entire vortex volume. For the Arctic, chlorine activation typically occurs in association with the formation of PSCs over only a small portion of the vortex. Nonetheless, a small cold vortex portion often results in substantial vortex-wide activation (e.g., Wegner et al., 2016). Frequently, an early sudden stratospheric warming (SSW), for example in January, causes the vortex to split or even break down, resulting in very weak chemical ozone loss. However, there are also cases such as winter 2012/2013 that started with a very cold December followed by a SSW in January in which significant ozone loss occurred (Manney et al., 2015).

At the end of the period of catalytic ozone depletion, the Arctic typically follows a pathway involving the predominant formation of $ClONO_2$ from active chlorine, as opposed to the Antarctic, where active chlorine is mainly converted into HCl. The pathway of chlorine deactivation depends on how low ozone mixing ratios fall (Crutzen et al., 1992; Douglass et al., 1995; Grooß et al., 1997; Müller et al., 1994). In Arctic winters with a cold and stable vortex, for example the winter 1996/1997 or winter 2010/2011, denitrification and ozone depletion cause chlorine deactivation to follow a more Antarctic-like pathway, that is, a faster formation of HCl than in more typical Arctic winters (Douglass & Kawa, 1999; Manney et al., 2011). In winter 2019/2020, which is considered here, this combination of factors also caused a similar evolution of chlorine deactivation (Manney et al., 2020).

Here we report on simulations using the model Chemical Lagrangian Model of the Stratosphere (CLaMS) which show unprecedented Arctic ozone depletion in the year 2020 (Dameris et al., 2021; Feng et al., 2021; Manney et al., 2020; Wohltmann et al., 2020) accompanied by a significant increase in surface UV radiation (Bernhard et al., 2020). The reported simulations indicate that the major causes of the severe ozone depletion reported in the Arctic in 2020 are the low stratospheric temperatures and the exceptionally stable polar vortex extending into spring (Lawrence et al., 2020).

2. Data Description

2.1. Aura-MLS

The observations made by the Microwave Limb Sounder (MLS) on board the Aura satellite are the main data set used in this study. Further details of the MLS measurements in Arctic winter 2019/2020 are reported by Manney et al. (2020). MLS makes its observations in limb-viewing geometry in the A-Train orbit, circling the Earth about 14 times per day and covering latitudes from 82°S to 82°N. We use MLS version 4.2 data (Livesey et al., 2020). Here observations of O_3, N_2O, HCl, H_2O, ClO, and HNO_3 are used for model initialization, boundary conditions, and comparison with the model results. The vertical resolution of the data in the lower stratosphere ranges from about 3 km (O_3, HCl, H_2O, ClO) to about 5 km (N_2O, HNO_3). The reported accuracy or systematic uncertainty in the lower stratosphere (100-22 hPa) is 5%–8% for ozone, 6% at 22 hPa to 44% at 100 hPa for N_2O, 0.2 ppbv for HCl, 4%–9% for H_2O, 1.0–2.4 ppbv for HNO_3, and 0.2–0.25 ppbv for ClO, respectively (Livesey et al., 2020). The precision of the data is of little consequence here as we mostly use averages over multiple profiles.

2.2. ACE-FTS

The Atmospheric Chemistry Experiment-Fourier Transform Spectrometer (ACE-FTS) on the SCISAT satellite is a Fourier transform spectrometer with high spectral resolution (0.02 cm^{-1}) operating from a wavelength of 2.2–13.3 μm employing a Michelson interferometer (Bernath et al., 2005). Since 2004, it has

observed around 30 profiles per day in solar occultation geometry with the majority of the measurements in high latitudes. The vertical resolution is about 3–4 km. Here we use version 3.6 data of O_3 and N_2O as well as the five main components of total inorganic nitrogen NO_y (NO, NO_2, N_2O_5, HNO_3, $ClONO_2$). The retrieval used in version 3.6 is described by Boone et al. (2013). Ozone measurements are in general agreement with other observations to within ±5% and have a small bias of +2% (Sheese et al., 2017).

2.3. Aura-OMI

The Ozone Monitoring Instrument (OMI) onboard the Aura satellite is a nadir-looking, push-broom solar backscatter spectrometer that measures the solar radiation back-scattered by the Earth's atmosphere and surface over the entire UV/VIS wavelength range from 270 to 500 nm (Levelt et al., 2006). OMI is the successor to the Total Ozone Monitoring Spectrometers (TOMS). Since 2004, OMI has provided high spatial resolution measurements on about 14 orbits per day with ground pixels of 13 × 24 km and a swath width of 2,600 km. This results in an almost global coverage of the distribution of the atmospheric ozone column on a daily basis. Ozone columns are derived by means of differential optical absorption spectroscopy (DOAS). The ozone columns show a 0.4% ± 0.6% bias with respect to ground-based stations (McPeters et al., 2008).

2.4. Ozone Sondes

We also present data from two balloon-borne ozone sondes that were launched in Ny Ålesund, Spitsbergen (78.9°N, 11.9°E, WMO station number 1004). The balloons were flown with an ECC ozone sonde together with a radiosonde RS41. Using standardized operating procedures the ECC-sondes yield an accuracy of about 5%–10% up to an altitude of 30 km (Smit et al., 2007). These measurements were made as part of an international ozone sonde campaign in 2019/2020 (Wohltmann et al., 2020).

3. Model Description

3.1. Model Setup

The simulations described here were performed using the CLaMS. Unlike in previous publications, the chemical transport model CLaMS here is driven by operational analyses by the European Centre for Medium Range Weather Forecasts (ECMWF). The vertical velocities were thus derived from heating rates calculated by an offline radiation module based on the Morcrette scheme (Morcrette, 1991; Zhong & Haigh, 1995) as in an earlier model setup (Konopka et al., 2004). The vertical model coordinate is the hybrid potential temperature ζ (Konopka et al., 2004; Pommrich et al., 2014) that is identical to the potential temperature above 100 hPa (above about $\theta = 400$ K) and corresponds to a terrain following σ-coordinate system below 100 hPa with a smooth transition. The model simulation described here starts on November 1, 2019 and runs until mid-April 2020. The model domain consists of the Northern Hemisphere with a horizontal resolution of 100 km. The vertical range spans from the surface to a potential temperature of 900 K divided into 32 levels with a variable resolution in the stratosphere ranging from 0.7 km at 9–12–1 km at the top layer, yielding about 820,000 air parcels in total.

The chemistry scheme used here has been described earlier (Grooß et al., 2011, 2018; McKenna et al., 2002). The chemical kinetics and absorption cross sections are based on current recommendations (Burkholder et al., 2015). A comprehensive stratospheric chemistry scheme is employed which includes a full set of heterogeneous reactions. The vertical re-distribution of NO_y and H_2O due to sedimenting nitric acid trihydrate (NAT) and ice particles is determined by Lagrangian NAT and ice particle tracking (Grooß et al., 2014; Tritscher et al., 2019). This algorithm allows denitrification and also dehydration to be represented in the model. Heterogeneous chemistry is calculated here only on liquid PSCs and aerosols. This assumption is justified as heterogeneous chlorine activation is dominated by liquid PSCs and aerosols. NAT particles have much lower particle number densities than liquid particles so the heterogeneous reaction rates for liquid particles exceed those for NAT (Portmann et al., 1996; Tritscher et al., 2021; Voigt et al., 2005; Ward et al., 2014; Wegner et al., 2012). NAT particles are important as they cause denitrification through their gravitational settling (e.g., Fahey et al., 2001; Solomon, 1999; Tritscher et al., 2021).

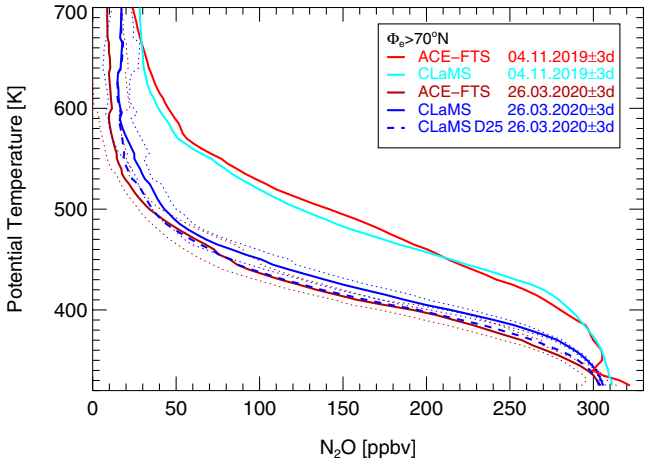

Figure 1. Atmospheric Chemistry Experiment-Fourier Transform Spectrometer (ACE-FTS) comparison: mean vortex ($\Phi_e > 70°N$) N_2O mixing ratios in the time frames 26 March ±3 days and 4 November ±3 days, respectively. The red and dark red lines show the average observed N_2O mixing ratio profile for November 2019 and March 2020, respectively. The dotted lines correspond to the standard deviation of the March measurements ($\pm 1\sigma$). Light and dark blue lines are from the Chemical Lagrangian Model of the Stratosphere simulation interpolated to ACE-FTS profile locations and are evaluated correspondingly. About 20 observed (and correspondingly simulated) profiles contribute to each shown line.

3.2. Initialization and Boundary Conditions

The chemical composition at the beginning of the simulation and the boundary conditions at the surface as well as at the top model layer at a potential temperature of 900 K are derived from a variety of data and model results. The procedure is similar to previous work (Grooß et al., 2014, 2018). Data from MLS were used within ±2.5 days of the initial time for O_3, HNO_3, H_2O, HCl, and N_2O. The observation locations were transferred to the initial time using CLaMS trajectories and averaged to a 2° latitude × 6° longitude grid. In the troposphere below a potential temperature of 350 K, the initialization of these compounds was taken from a multi-annual CLaMS simulation with a simplified chemistry setup (Pommrich et al., 2014). For total inorganic nitrogen (NO_y), chlorine (Cl_y) and bromine (Br_y), tracer correlations with N_2O were used as listed in the supporting information. NO_y was derived from ACE-FTS from the sum of the observations of HNO_3, NO, NO_2, N_2O_5, and $ClONO_2$ between October 1 and November 21, 2019. The sum of these NO_y compounds correlates well with N_2O, with different correlations for different latitude ranges (tropics, sub-tropics, mid-latitudes, higher, and polar latitudes). The NO_y initialization is based on the correlations in these five latitude ranges, which are listed in the supporting information. Cl_y and Br_y were initialized using correlations with N_2O derived from balloon observations, updated from Grooß et al. (2011) as described in the supporting information. The partitioning within these chemical families was taken from a 2-D reference model (Grooß, 1996) with updated boundary conditions (WMO, 2018).

The chemical composition at the upper boundary at the potential temperature level of 900 K was calculated using the same data sources. Twice a month at this level, the data described above are mapped and averaged into bins of equivalent latitude Φ_e (Butchart & Remsberg, 1986; Lary et al., 1995). Thus the chemical composition at the upper boundary is determined. Simulations have been performed using this setup for several Arctic winters since 2010.

4. Results

The CLaMS simulation aims to reproduce the processes involved in Arctic stratospheric ozone depletion during winter 2019/2020. We analyze the observations and the model results in the polar vortex using the concept of equivalent latitude (Butchart & Remsberg, 1986). In the simulation, NAT particles start to form on November 16, 2019. The period of chlorine activation in the stratosphere was exceptionally long (Manney et al., 2020). ClO_x/Cl_y averaged over the polar vortex core ($\Phi_e > 75°N$) exceeded 50% at a rather early stage on 14 December at a potential temperature between about 490 and 540 K. Thus, some ozone depletion already occurred in December (compare Figure 4 below). Chlorine activation in 2020 lasted until 22 March, and the polar vortex remained stable into the month of April (Lawrence et al., 2020).

4.1. Descent in the Polar Vortex

To evaluate the simulation results, it is essential to demonstrate the ability of the model to reproduce atmospheric observations. One important aspect of the simulation is whether the transport and dynamics are represented correctly. In particular, the diabatic descent of air inside the polar vortex should be realistic. Diabatic descent in any given winter determines not only the ozone mixing ratios at a given potential temperature level in spring, but also the available Cl_y (Strahan et al., 2014). We therefore evaluated the simulated descent of vortex air by comparing the simulation with ACE-FTS N_2O data, which have better vertical resolution and accuracy in the lower stratosphere than the MLS measurements of N_2O. Figure 1 shows a comparison of ACE-FTS N_2O profiles for two periods (1–7 November 2019 and 23–29 March 2020) in the vortex ($\Phi_e > 70°N$) and the corresponding CLaMS data at the observation locations. These periods

correspond to the model initialization and the latest date with a sufficient number of ACE-FTS observations at latitudes within the polar vortex. As only about 20 observed profiles contribute to each of the averages shown, their mean value and scatter may not be representative for the entire vortex, but it is still the best available information for investigating the deviation of the simulation with respect to the observations. The solid lines show the mean mixing ratio profiles and the dotted lines show the standard deviations. The CLaMS simulation shows weaker descent than observed between early November and late March. For example, for 200 ppbv N_2O, the simulated change is 54 K instead of the observed 64 K. For 100 ppbv N_2O, the simulated descent is 68 K instead of the observed 90 K. This difference in vertical displacement is on the order of the model vertical resolution. Because of this discrepancy, we introduced a sensitivity simulation, labeled "D25", which is designed to better represent the observed N_2O vertical profile in the vortex, that is, which better represents the observed diabatic descent. This is achieved by artificially increasing the diabatic cooling rates north of 60°N by 25%. The dashed blue line in Figure 1 shows that the diabatic descent is represented well in the D25 simulation. However, since this artificial modification causes a not self-consistent wind field, the aim of the D25 simulation is only to indicate the sensitivity of the model results with respect to the diabatic descent rate.

4.2. Ozone Depletion

The focus of this study is on the simulation of ozone depletion in the Arctic in 2020. To evaluate the simulation results, they are compared with ozone observations. First, the overall development of ozone is compared with MLS data. As the MLS measures about 3,500 profiles per day, the comparison is performed in such a way that similar air-masses are averaged. To do so, both the data and the simulations are averaged on a daily basis into equivalent latitude and potential temperature bins. The width of the equivalent latitude bins is chosen in such a way that they correspond to equal geographical areas. Figure 2 displays different illustrations of these averages for MLS measurements. Panel a shows the temporal development of the vortex core average profiles for equivalent latitudes $\Phi_e > 75$°N; panel b shows the temporal development of the mixing ratio at the potential temperature level of 450 K and as a function of equivalent latitude. Panels c and d show equivalent latitude/potential temperature cross sections for two particular days—31 January and 29 March.

These 2 days were selected as representative days in the early phase and toward the end of the ozone depletion period, respectively. Most of the plots below show results for 29 March, as the lowest ozone mixing ratios were found around this time. Figure 3 shows the development of ozone corresponding to Figure 2, but derived from the CLaMS simulation. For this comparison, the model data were not interpolated to MLS locations but were averaged directly into the same bins. This procedure is justified by the high spatial coverage of MLS. Although there are some small differences, the ozone depletion over winter and spring is well reproduced by the simulation. The lowest ozone mixing ratios in the stratosphere are seen at a potential temperature between 400 and 500 K toward the end of March. The gradients of ozone at the edge of the polar vortex are reproduced well. The lowest MLS mean vortex core ($\Phi_e > 75$°N) ozone mixing ratio reached is 0.21 ± 0.28 ppmv (mean value ± standard deviation) at 450 K on 27 March. The corresponding ozone mixing ratio from the CLaMS simulation in these air masses is 0.29 ± 0.26 ppmv.

Figure 4 shows the simulated ozone mixing ratios in the vortex core ($\Phi_e > 75$°N) versus time at four different potential temperature levels together with the corresponding MLS observations. Dashed lines depict the evolution of the passive ozone tracer. The D25 simulation shows the sensitivity with respect to the vertical descent rate. Stronger vertical descent increases Cl_y and thus the chemical ozone depletion but at the same time also increases ozone itself since ozone increases with altitude. The latter effect is visible in the increase in passive ozone.

At 450 K, the simulation reproduces the temporal development and especially the observed low ozone mixing ratios, both for the reference simulation and for the D25 simulation with enhanced vertical descent. At 400 K, the ozone mixing ratio in April in the reference simulation is lower than the MLS observations by about 0.2 ppmv. In the D25 simulation at 400 K, the vortex core ozone mixing ratio after late March decreases below the reference simulation in early March reaching about 0.1 ppmv below the reference simulation in April, even though the simulated passive ozone is larger by about 0.2 ppmv. This additional ozone depletion of 0.3 ppmv is due to the Cl_y increase caused by the artificially increased descent. At 550 K, the

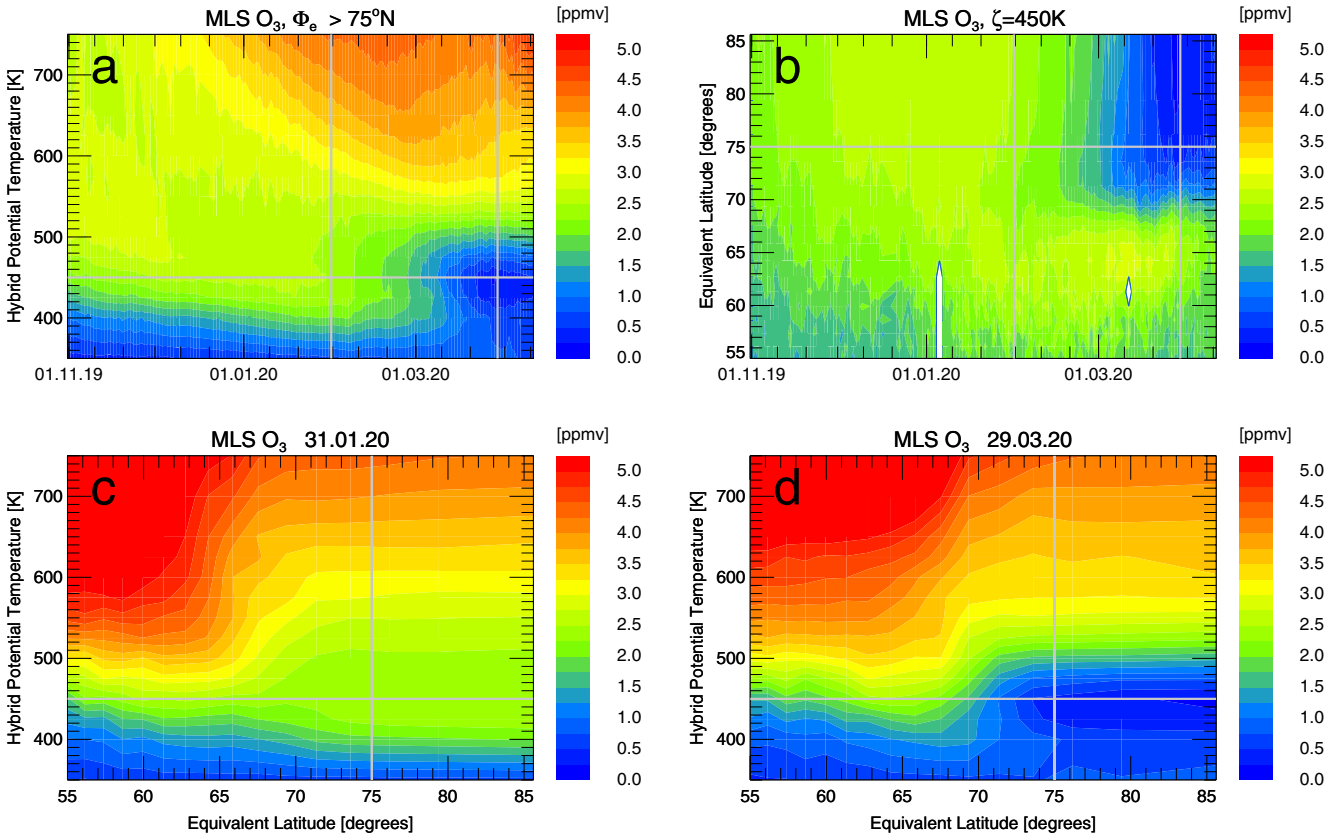

Figure 2. Microwave Limb Sounder ozone observations averaged in equivalent latitude/potential temperature space. Panel a shows the vortex core ($\Phi_e > 75°N$) average as a function of potential temperature and time. Panel b shows the observations at the potential temperature of 450 K as a function of equivalent latitude and time. Panels c and d show equivalent latitude/potential temperature cross sections for two specific days—31 January and 29 March. Gray lines overlaid in the plots indicate the slices through the data, as displayed in the other panels.

simulated ozone depletion is likely an under-estimation, yielding larger ozone mixing ratios than observed by about 0.3 ppmv by mid-March. This discrepancy is about 0.6 ppmv for the D25 simulation with increased descent. As the simulation D25 is based on inconsistent wind fields, it should only be used to demonstrate the model's sensitivity to descent rate, a critical parameter. The differences between observations and model results arise partly because of the difficulty to accurately reproduce the large vertical gradients of the ozone profiles. However, the shown discrepancy is still small compared to the ozone depletion itself derived as the difference between the simulated ozone and the passive ozone tracer.

The simulated ozone profiles in spring 2020 were compared with a variety of observations. Figure 5a shows the average vortex ozone profile observed by ACE-FTS between 23 and 29 March. The corresponding CLaMS simulations were evaluated at the ACE-FTS tangent point locations. Dotted lines show the standard deviation of the observed mixing ratios. Since only about 20 observed profiles contribute to this vortex core average, their mean value and scatter may not be representative for the entire vortex, but similar to the N_2O comparison in Figure 1, these data are a good measure of the quality of the simulation results. At a potential temperature of around 450 K, the simulations show lower ozone mixing ratios (by 0.35 ppmv) than those observed by ACE-FTS, but measured and modeled profiles agree within the combined standard deviations. Figure 5b shows the corresponding comparison with MLS ozone data for 29 March for the vortex core $\Phi_e > 75°N$. Instead of about 20 profiles as in the case of ACE-FTS, about 230 MLS profiles contribute to this vortex-core average, providing a much better coverage of the vortex core. The dashed blue line corresponds to the model data convolved with the MLS averaging kernel. Here the minimum ozone near 450 K is well reproduced. However, for equivalent latitudes near the vortex edge, the model under-estimates somewhat the minimum ozone mixing ratio (see Figure S9 of the supporting information). The Lagrangian model CLaMS has been shown to better reproduce trace species gradients near the vortex edge than a comparable

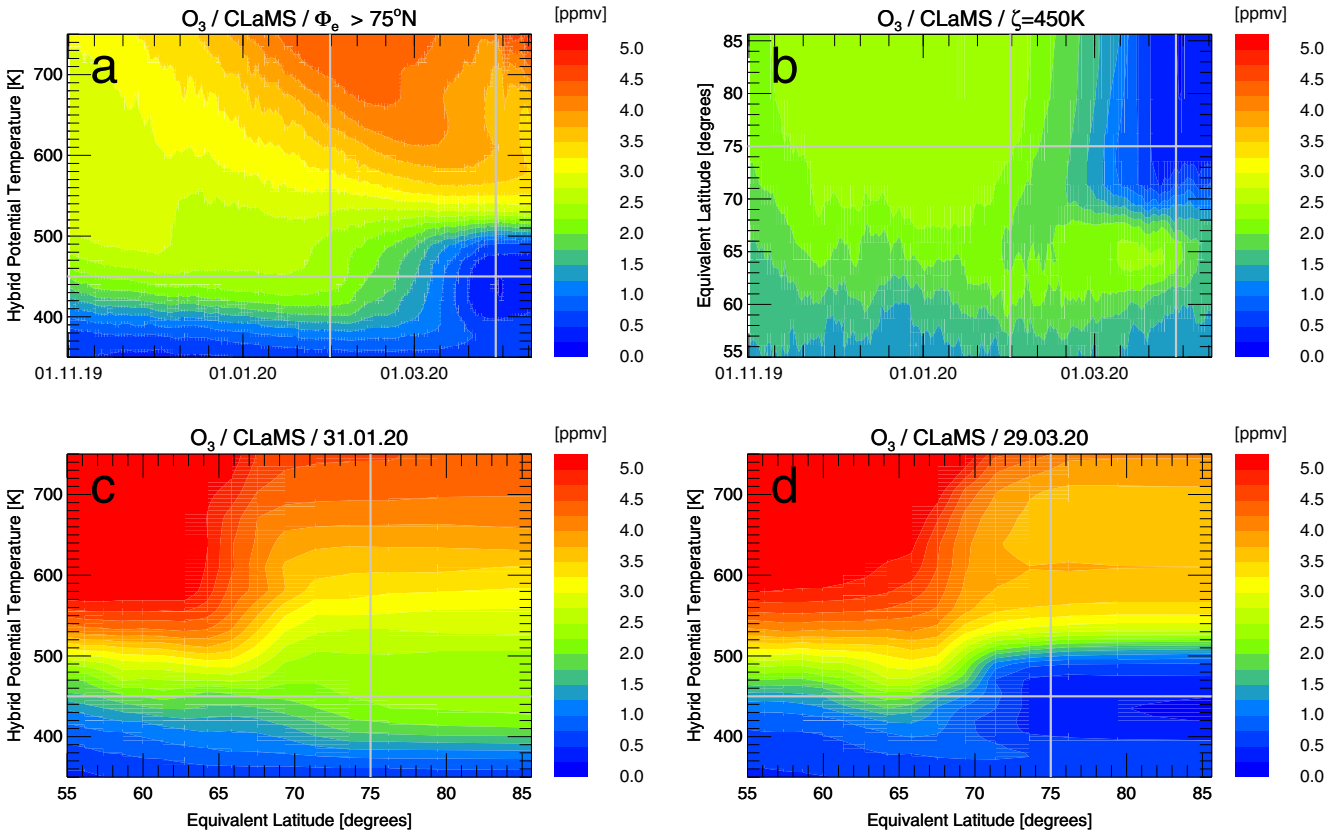

Figure 3. Chemical Lagrangian Model of the Stratosphere simulation of ozone plotted in accordance with Figure 2.

Eulerian model setup (Hoppe et al., 2014), but still deviations from observed distributions remain. For the simulation shown here, the deviation between MLS and simulation results for the vortex edge is consistent with the difference between the simulation results and the ACE-FTS observations, which are predominantly located near the vortex edge.

Furthermore, Figures 5c and 5d show the comparison of CLaMS results with measurements by two balloon-borne ozone sondes launched from the Ny Ålesund station on 29 March and 12 April. Between 400 and 500 K, the simulation and the ozone sonde measurements are in good agreement; especially around 450 K, the comparison of the minimum ozone mixing ratio between the simulated and observed ozone mixing ratios is better than for the satellite data.

Although the minimum ozone mixing ratio at a potential temperature around 450 K has been simulated quite well, it is notable from the comparisons with all different data sets that the simulated ozone mixing ratio around 575 K is over-estimated by the simulation, whereas it is somewhat under-estimated below about 400 K. The reasons for these discrepancies remain unclear. A comparison of ClO and HCl data shows that the model might underestimate the vertical extent of the chlorine activation, placing the upper edge of the activated region at a lower altitude than is observed (compare supporting information Figures S1, S2, S4–S6), but the limited vertical resolution of the data prevents a definitive determination.

In the following, we discuss the simulated chemical ozone change. The chemical ozone change (Figure 6) is calculated as the difference between the simulated ozone and a passive ozone tracer that has identical initialization and boundary conditions and transport as the simulated ozone, but no chemical change. The maximum ozone depletion calculated in this way for the vortex core average (Φ_e > 75°N) is 2.74 ppmv, which was reached on 30 March at the potential temperature of 470 K. After that day, this value remained approximately constant until mid-April, indicating no additional chemical ozone loss but also no significant mixing with mid-latitude ozone-rich air. This magnitude is quite comparable with the Match ozone loss reported by Manney et al. (2020). The simulated maximum ozone loss is located at a somewhat higher

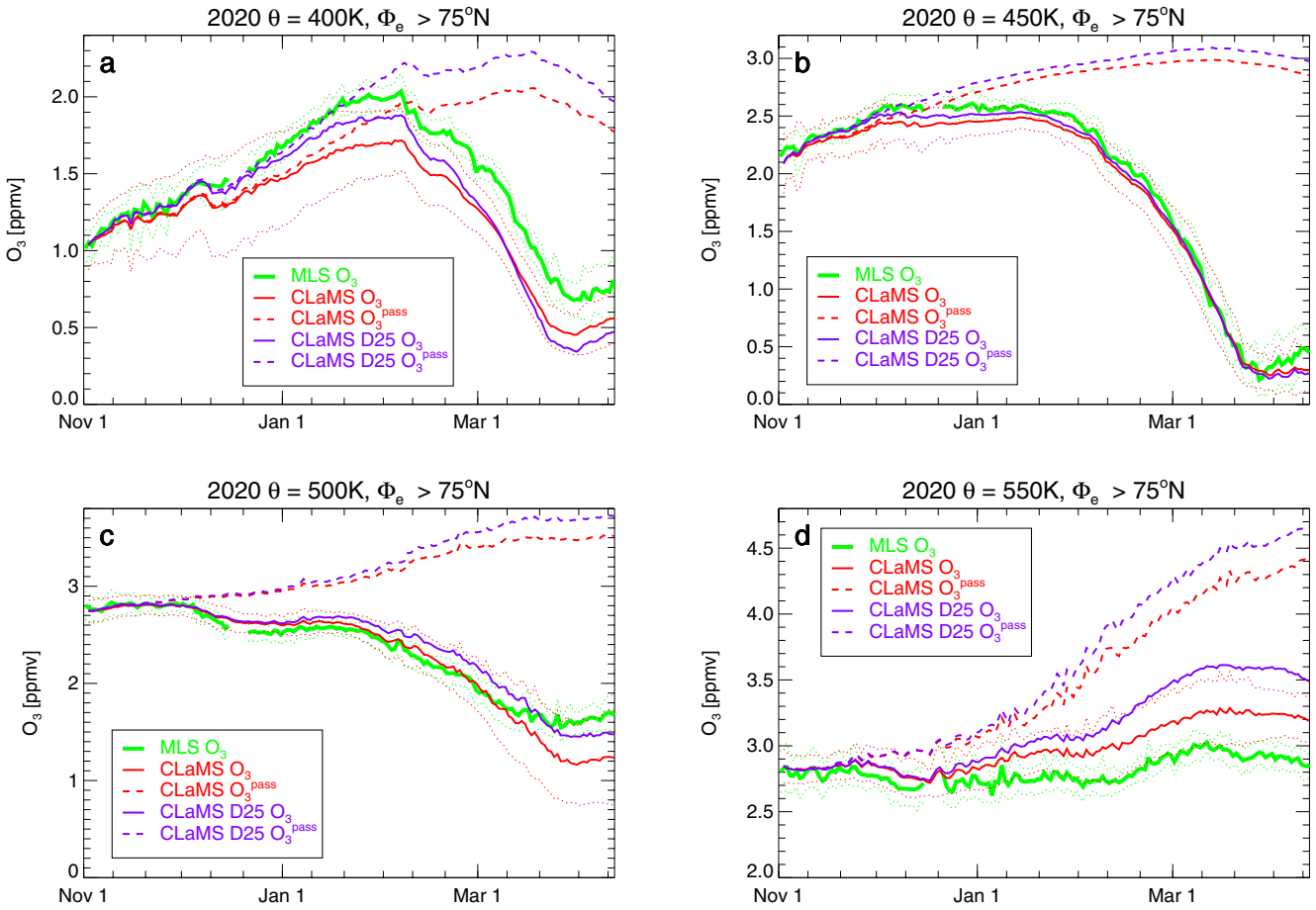

Figure 4. Mean ozone mixing ratio at the potential temperature of 450 K for the equivalent latitude range of $\Phi_e > 75°N$. Microwave Limb Sounder observations are shown as a green line and corresponding Chemical Lagrangian Model of the Stratosphere results as a red line. The red dashed line depicts the passive ozone tracer. Dotted colored lines show the standard deviations $\pm 1\sigma$ of the observations and simulations within the given equivalent latitude range. The violet line shows ozone for the D25 simulation with artificially enhanced descent rates.

potential temperature than in the Match estimate (470 K instead of about 440 K). The reason for this is as yet unclear.

In the middle stratosphere at mid-latitudes above about 600 K, this simulation also indicates ozone depletion (Figure 6c). However, the most important ozone-depletion reactions in this region are NO_x-induced catalytic cycles. Due to the shorter lifetime of mid-latitude ozone compared to high latitudes, the simulated mid-latitude ozone mixing ratios are mostly determined by chemical production and loss rather than by transport processes (see e.g., Figure 11 of Garcia & Solomon, 1985). Thus, the use of a passive ozone tracer to calculate chemical ozone loss is inappropriate for mid-latitude air masses above about 600 K. These mid-latitude aspects will not be discussed further in this paper as our focus is on chlorine-catalyzed ozone loss in the polar region.

With respect to the variability of surface UV radiation due to polar ozone depletion, the total ozone column is important. To calculate the simulated total ozone column, the ozone column above 900 K potential temperature is added to the column over the vertical model domain considered here. The column above 900 K amounts to about 30 Dobson Units (DU) as determined from a climatology dependent on the equivalent latitude and time of year (Grooß & Russell, 2005). Employing this estimate of the ozone column above 900 K, the geographical distribution of ozone columns is well reproduced by the simulation. Figure 7 shows a comparison of the geographical distribution of ozone columns from Aura-OMI and CLaMS for 29 March. The OMI data are observed and accumulated over a 24-h period (resulting in a discontinuity on the date line), while the model data are displayed for the synoptic time 12:00 UTC. This comparison shows the ability of

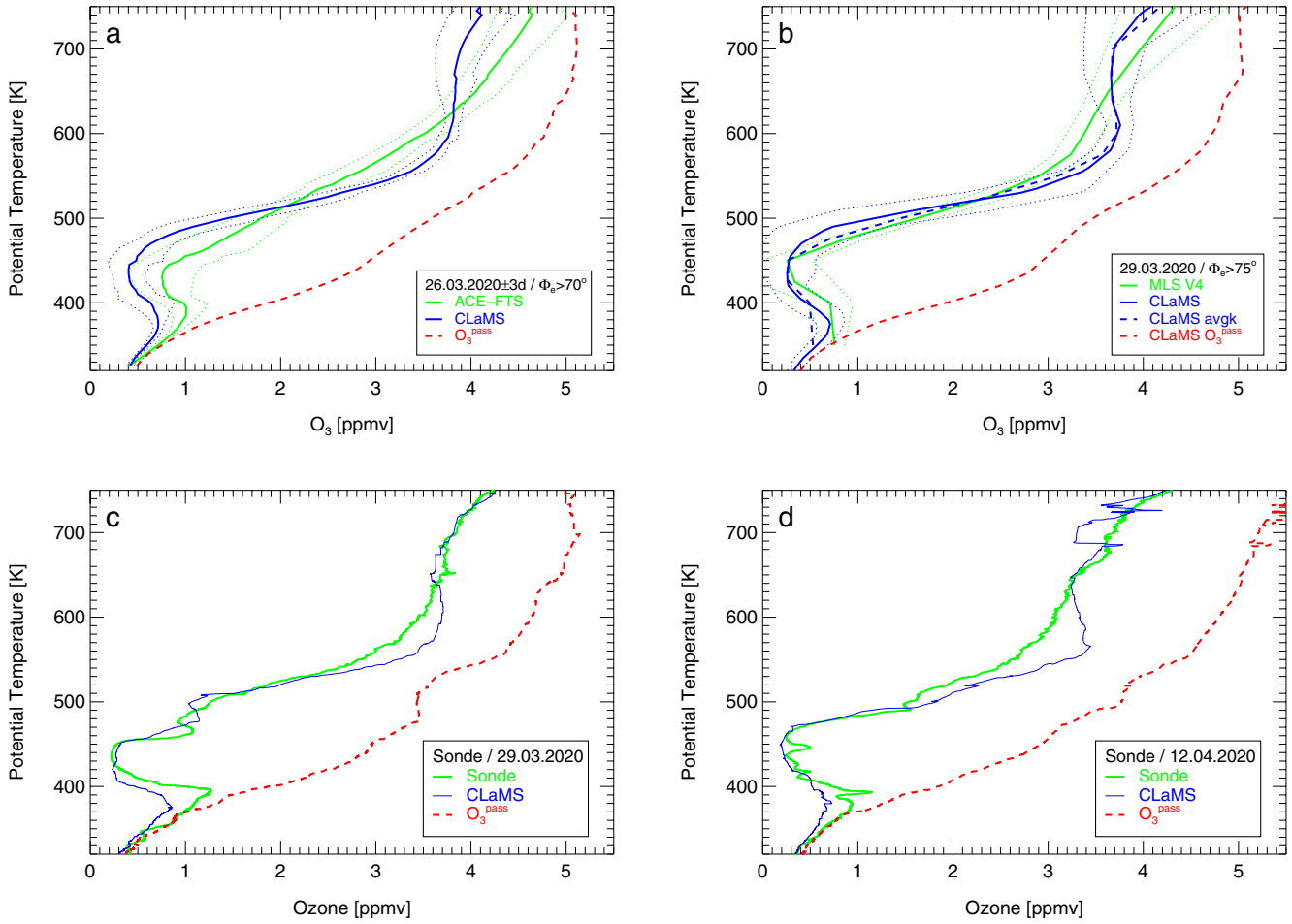

Figure 5. Simulated profiles of ozone mixing ratios compared to observations. (a) Atmospheric Chemistry Experiment-Fourier Transform Spectrometer vortex ($\Phi_e > 70°$N) average in the time frame 26 March ±3 days; (b) Microwave Limb Sounder (MLS) vortex core ($\Phi_e > 75°$N) average for 29 March; (c, d) single ozone sondes from Ny Ålesund (78.9°N, 11.9°E) from 29 March and 12 April. The green lines correspond to the (mean) observations. Dotted lines correspond to the standard deviation of the measurements (±1σ). Blue lines are from the Chemical Lagrangian Model of the Stratosphere (CLaMS) simulation interpolated to measured profile locations and are evaluated correspondingly. In the case of MLS (b), the blue dashed line corresponds to the CLaMS data convoluted with the MLS averaging kernel. The red dashed line marks the mixing ratio of the passive ozone tracer.

the CLaMS simulation to accurately reproduce the structure and the gradients in the ozone distribution. Inside the vortex, the so-calculated total ozone column is about 10–15 DU larger than the OMI data (see Figure S10 of the supporting information).

The strongest ozone depletion occurs in the vortex core ($\Phi_e > 75°$N) in the partial column over the potential temperature range between 350 and 600 K. The average development of the simulated depletion over this region is shown in Figure 8. For this volume, the maximum partial column ozone depletion of 143 DU was reached on 4 April. Toward the end of this time period there is some variability in the deduced ozone depletion values because of the beginning of vortex breakup. This is because the ozone-depleted air masses are no longer congruent with contours of PV (or Φ_e). In the D25 sensitivity simulation with artificially increased polar descent rates, the uncertainty of the partial column ozone loss estimate is also evident. Increased descent causes an increase of the passive ozone tracer but, more importantly, it also leads to an increase in Cl_y. Since the ozone mixing ratios at lower altitudes contribute significantly to the column, the derived partial ozone column depletion for the D25 simulation is 160 DU, which is 17 DU more than in the reference simulation. Thus, there is some uncertainty in the derived partial ozone column depletion. However, the fact that the absolute total ozone column distribution is simulated well (Figure 7) strengthens the credibility of the simulation results.

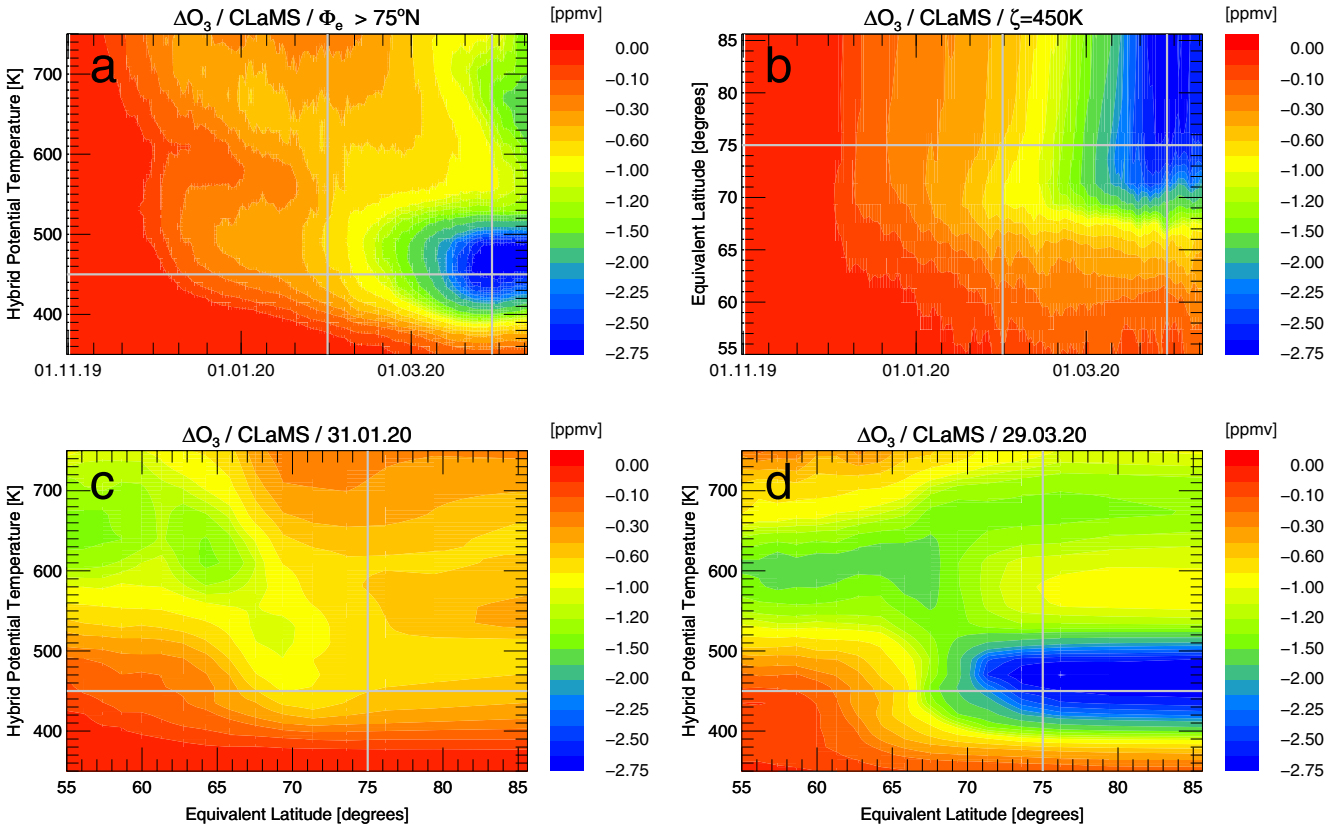

Figure 6. Simulated chemical ozone depletion determined by the difference between simulated ozone and the passive ozone tracer averaged in equivalent latitude and potential temperature bins. The results are displayed in the same style as in Figures 2 and 3.

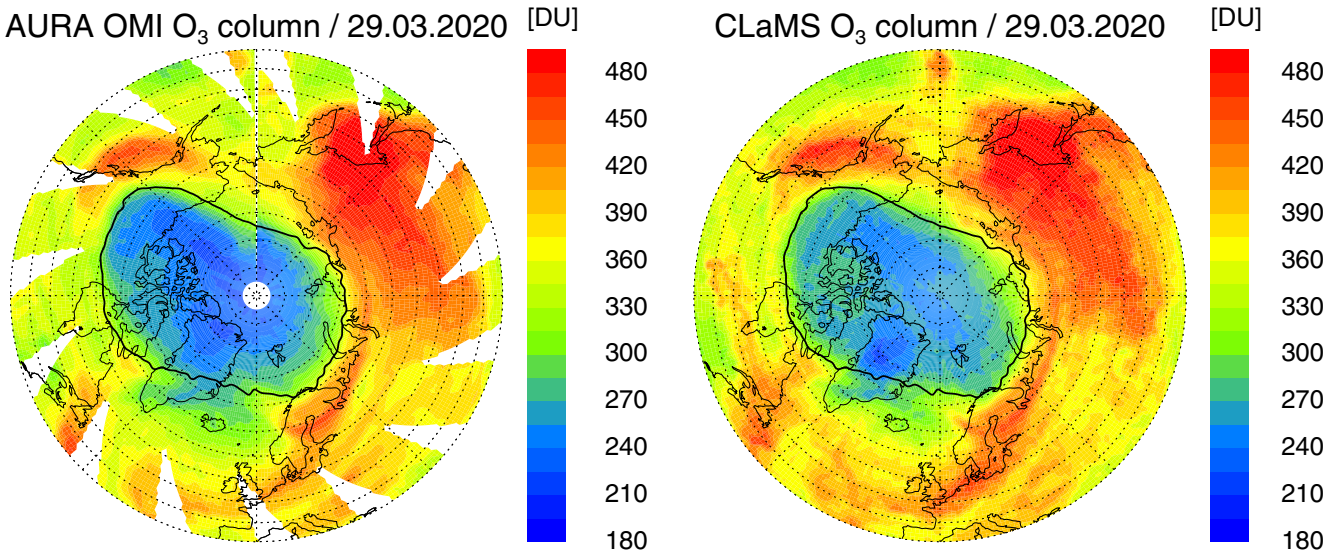

Figure 7. Ozone columns for 29 March (left) from Aura-Ozone Monitoring Instrument and (right) from the Chemical Lagrangian Model of the Stratosphere simulation. The solid line marks the vortex edge according to Nash et al. (1996) at the potential temperature of 450 K (roughly corresponding to $\Phi_e = 70°$N). Equivalent latitude development of the vortex edge is shown in Figure S11 of the supporting information.

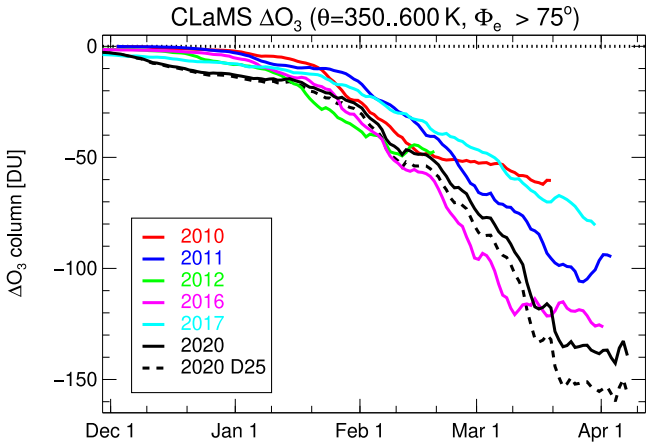

Figure 8. Development of simulated partial ozone column depletion for the potential temperature between 350 and 600 K averaged over the vortex core ($\Phi_e > 75°$N). Comparable Chemical Lagrangian Model of the Stratosphere simulations for other years of significant Arctic ozone depletion including 2011 and 2016 are also shown. The simulated column ozone depletion in the vortex core on April 4, 2020 is 143 DU. The black dashed line shows the results from the D25 simulation with artificially enhanced descent rates (160 DU ozone loss on 4 April).

For comparison, Figure 8 also shows the simulated depletion of ozone partial column for comparable CLaMS simulations for years with significant Arctic ozone depletion in the previous decade, including 2011 and 2016—the years that are known for the largest Arctic ozone depletion before 2020. The corresponding maximum ozone partial column depletion for the other cold Arctic winters determined by CLaMS simulations was 62 DU for 2010, 106 DU for 2011, 49 DU for 2012, 126 DU for 2016, and 81 DU for 2017. The calculated partial column ozone depletion in 2020 clearly exceeds the values for 2011 and 2016 and all other previous years. Thus 2020 had the largest simulated Arctic ozone partial column depletion within all available CLaMS simulations since 2010. Wohltmann et al. (2020) derive a partial column depletion of 124 ± 11 DU from sonde observations and passive ozone tracer simulations for the potential temperature range 370–550 K. This number is derived as an average for all sonde observations that fall below 0.2 ppmv within this vertical range. Their simulated vortex-average partial column ozone loss (370–550 K) is 126 DU. For the same vertical range, CLaMS partial ozone column depletion on 4 April is very similar at 131 DU, which includes a 2.5 DU loss in November that was not considered by Wohltmann et al. (2020).

For 2011, ozone depletion restricted to the potential temperature range 350–550 K in early April was calculated here as 101 DU, somewhat lower than the 112 DU reported by Kuttippurath et al. (2012) for this vertical range. Over the potential temperature range of 380–550 K, ozone loss was calculated as 95 DU, lower than the 120 DU reported by Sinnhuber et al. (2011) for mid-April. About 10 DU of the latter difference is due to the fact that the 2011 CLaMS run stopped at the end of March and thus did not simulate the ozone depletion that occurred in early April 2011. Wohltmann et al. (2020) derive a partial column ozone loss of 133 DU (370–550 K) for 2011, which is more than the ozone loss for 2020. However this value is inconsistent with our simulations (97 DU, 370–550 K) and other publications (95 DU by Isaksen et al., 2012 and 99/108 DU by Adams et al., 2012) besides the studies mentioned above (Kuttippurath et al., 2012; Sinnhuber et al., 2011).

As indicated above, the derived ozone depletion in 2020 exceeds the ozone depletion for previous Arctic winters including 2011. Although the partial column ozone depletion in the Arctic in 2020 reached record or near-record levels, it was still well below typical Antarctic values. For example, in the simulation for Antarctic spring 2011 (Grooß et al., 2018), the simulated maximum partial ozone column depletion in the lower stratosphere vortex core ($\Phi_e > 75°$S, 350–600 K) is 228 DU on 14 October.

4.3. Initial Chlorine Activation

Although the main aspects of polar chlorine activation and the resulting catalytic ozone loss are established (WMO, 2018), there are scientific questions on these issues that have not yet been resolved. In particular, HCl depletion has been observed in the cold and dark early winter polar vortex which cannot be reproduced using the processes currently implemented in models (Grooß et al., 2018). This effect is most pronounced in the Southern Hemisphere, but has also been seen in the 2016 Arctic winter (Grooß et al., 2018). It is also observed here for the year 2020 (Figure 9), but to a lesser extent than in the simulation for the Arctic winter 2015/2016. At 500 K, the HCl mixing ratios in the simulation for late December and January do not reach the low observed values (Figure 9). The discrepancies on other levels are smaller (compare Figures S1, S2 and S12 in the supporting information). The smaller discrepancy compared to 2016 is likely due to the earlier onset of chlorine activation in late November 2019.

4.4. Chemistry During the Termination of Ozone Depletion

In simulations, the development of individual air masses with extremely low ozone mixing ratios cannot be well simulated when mixing is over-estimated in a numerical model, for example when numerical

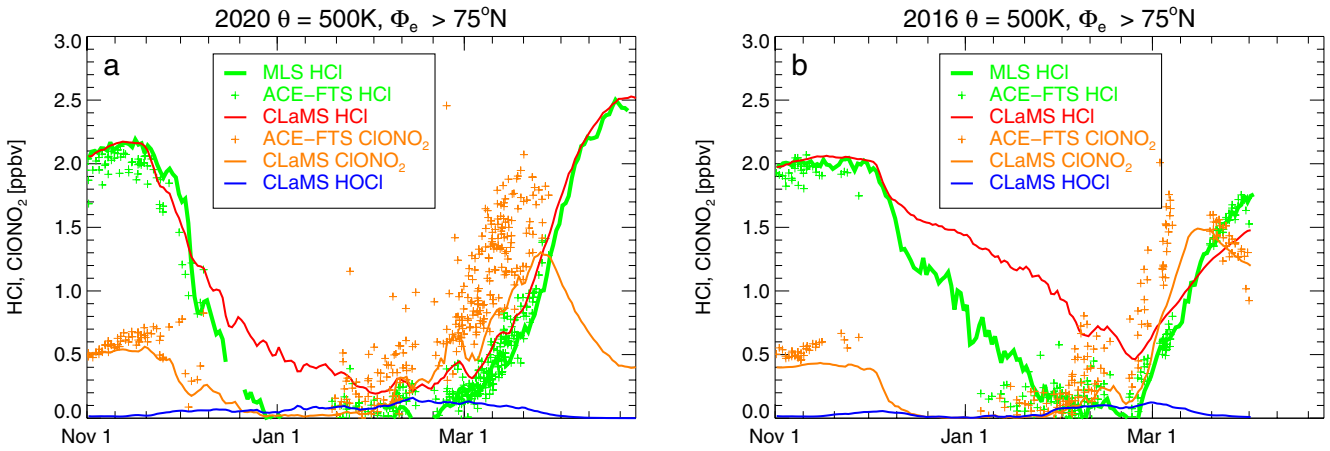

Figure 9. Vortex core ($\Phi_e > 75°N$) average HCl, $ClONO_2$, and HOCl mixing ratios at a potential temperature of 500 K simulated by Chemical Lagrangian Model of the Stratosphere and HCl observed by Microwave Limb Sounder. Individual $ClONO_2$ observations by Atmospheric Chemistry Experiment-Fourier Transform Spectrometer (ACE-FTS) are also shown as orange plus signs. Due to the sparsity of these data, no averages of ACE-FTS $ClONO_2$ are shown. (a) Current simulation for 2019/2020 and (b) simulation for 2015/2016 by Grooß et al. (2018). In 2016, this average only corresponds to the vortex core until mid-March (see Figure S11).

diffusion is too strong. The Lagrangian simulations shown here have the advantage of following individual air masses for some time without mixing. Lagrangian simulations allow the low Antarctic ozone mixing ratios observed to be reproduced (Grooß et al., 2011). In the current simulation for the Arctic in 2020, the simulated ozone mixing ratios did not quite reach the lowest levels reported for the Antarctic ozone hole (e.g., Solomon et al., 2005), where chemical ozone depletion can continue until extremely low ozone mixing ratios of the order of 10 ppbv have been reached (Grooß et al., 2011). The lowest simulated ozone mixing ratio in the polar lower stratosphere (38 ppbv) was reached on March 24, 2020 (84°N, 131°E, θ = 439 K). It is very unlikely that the model reproduces the exact location and mixing ratio of the ozone minimum in the real atmosphere. Nevertheless, this individual air parcel is useful here to analyze chlorine deactivation. This parcel was not affected by the CLaMS mixing algorithm for 50 days. The temporal development along this air parcel was reconstructed by exactly repeating the simulation for this air parcel only but saving more output details. Figure 10 shows the temporal development of ozone and chlorine compounds of this air parcel during the termination phase of ozone depletion. For an extended period—from about mid-February to early March—ClO_x levels remain strongly elevated in this air parcel, while the mixing ratios of HCl, $ClONO_2$, and HOCl remain very low.

For typical Arctic ozone mixing ratios, the dominant fraction of the active chlorine species undergoes deactivation into $ClONO_2$ through the ClO + NO_2 reaction (Douglass et al., 1995; Müller et al., 1994). For previous cold Arctic winters/springs, a chlorine activation pathway into HCl for air masses with low ozone was reported for Arctic winters/springs in 1997 (Douglass & Kawa, 1999), 2000 (Wilmouth et al., 2006), 2006 (Santee et al., 2008), and 2011 (Arnone et al., 2012; Manney et al., 2011). This is also the case for winter/spring 2020 (Manney et al., 2020). The CLaMS simulation similarly shows more typical Antarctic behavior as low ozone mixing ratios—almost comparable to Antarctic values—are reached, allowing deactivation into HCl to occur (Douglass et al., 1995; Grooß et al., 2011; Müller et al., 2018).

Chlorine activation in the atmosphere is likely dominated by liquid PSCs and aerosol particles (e.g., Portmann et al., 1996; Tritscher et al., 2021), which is also the assumption in the model runs presented here (see Section 3.1). It is well known that the chlorine activation rate has a strong temperature dependence, for example, the dominant chlorine activation reaction $ClONO_2$ + HCl shows an increase of a factor of 10 for a temperature decrease by 2.3 K (see e.g., Figure 1 of Wegner et al., 2012). As the temperature of the selected air parcel varies by roughly 10 K along its trajectory, Figure 10 illustrates the periods with and without a significant chlorine activation rate: periods corresponding to a first order heterogeneous reaction rate of reactions with HCl larger than 1 d^{-1} are depicted by gray shading. As temperatures decrease below about 194–195 K the first order HCl depletion rate by the reaction with $ClONO_2$ or HOCl increases above 1 d^{-1}

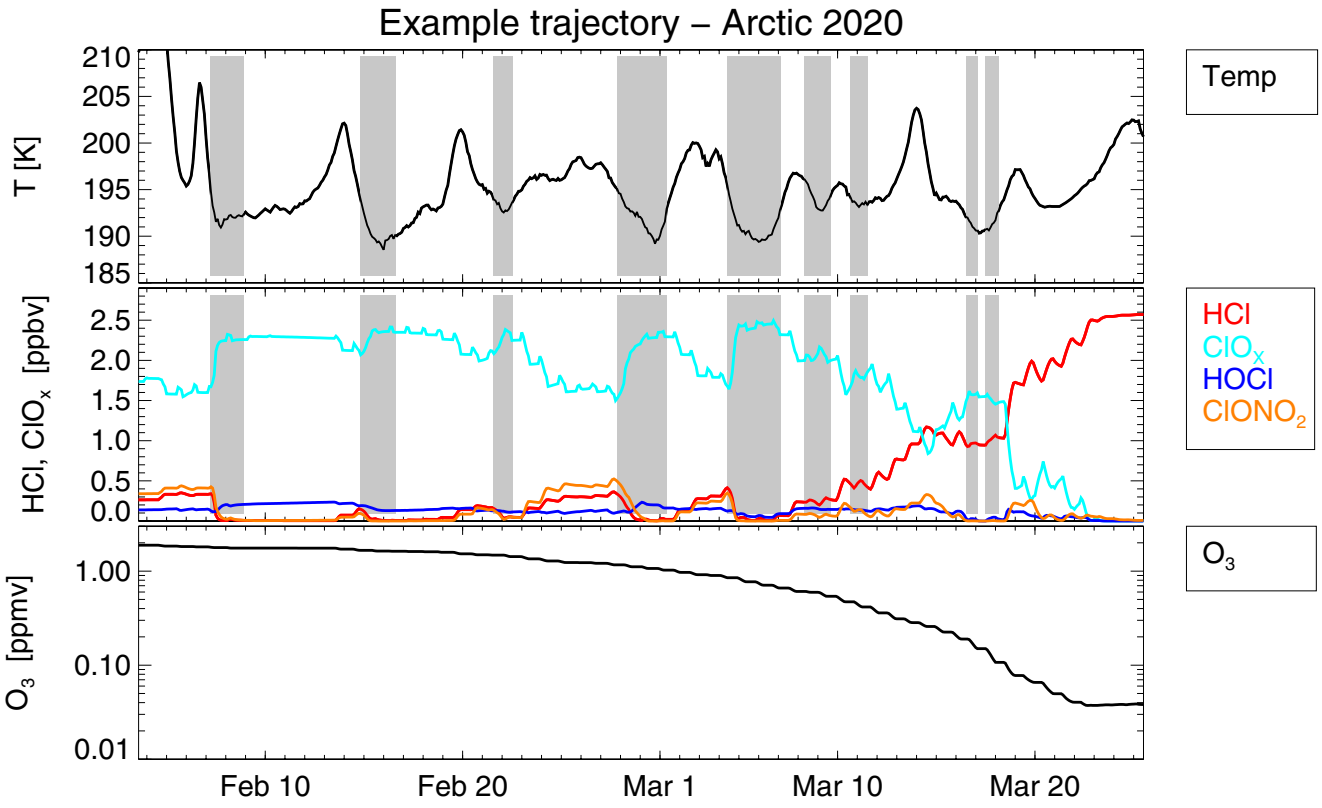

Figure 10. Fifty day development of one example air parcel trajectory from the CLaMS simulation that is not affected by mixing over the time period shown. The top panel shows the temperature along the air parcel trajectory (black). The periods when heterogeneous HCl loss rates ($k_{HCl + ClONO2}$ [$ClONO_2$] + $k_{HCl + HOCl}$ [HOCl]) are larger than 1 day^{-1} are marked as gray shaded areas. The middle panel shows the mixing ratio of the chlorine compounds HCl, $ClONO_2$, ClO_x (= ClO + 2 × Cl_2O_2 + 2 × Cl_2) and HOCl. Ozone is shown in the lowest panel on a logarithmic ordinate. The minimum ozone mixing ratio on 24 March (84°N, 131°E, θ = 439 K) is 38 ppbv.

despite the low mixing ratios of the reactants. However, in late March because of the low ozone mixing ratios this heterogeneous HCl depletion rate is counter-acted by fast chlorine deactivation into HCl. As is the case in the Antarctic, chlorine deactivation into HCl in the Arctic in 2020 already begins at a time (early March) when PSCs and liquid aerosol particles which allow heterogeneous chlorine activation to occur are still present. As the ozone mixing ratio did not decrease to values as low as in the Antarctic (Grooß et al., 2011; Solomon et al., 2005), the deactivation into HCl occurs over a longer time scale of about 2 weeks for this specific air parcel (Figure 10).

The chlorine deactivation into HCl is also present on a vortex-wide scale. The simulated vortex core averages for HCl and $ClONO_2$ ($\Phi_e > 75$°N) at a potential temperature of 500 K are shown in Figure 9a together with the corresponding MLS HCl data. ACE-FTS observations of $ClONO_2$ are also shown as individual points and not as an average, since the sparse coverage of ACE-FTS observations is not likely to be representative for the entire vortex. The rate of increase of vortex-averaged HCl mixing ratios in late March 2020 is lower than for the example given of the air parcel with the lowest ozone mixing ratio found in the simulation (Figure 10) since the HCl increase rate is largest for the lowest ozone mixing ratio (Grooß et al., 2011). Furthermore, in the vortex average for the potential temperature of 500 K, an HCl increase up to about 2.5 ppbv in mid-April is simulated, consistent with the HCl observations. The formation of $ClONO_2$ is also simulated in the model in February and March, but the vortex average is under-estimated compared to ACE-FTS $ClONO_2$ observations. This is likely in part due to the ACE-FTS sampling with a better coverage toward the vortex edge, where $ClONO_2$ abundances are larger, as noted for example by Santee et al. (2008) and evident in Figures of the supporting information. Figure S12 that shows simulated $ClONO_2$ for both vortex core average and individual points evaluated at observation locations. As in the chlorine deactivation phase of the unusual Antarctic winter 2002 (Grooß et al., 2005), chlorine deactivation in different areas follows here

different pathways that are mainly determined by the value of the ozone mixing ratio. The formation of both $ClONO_2$ and HCl at different locations has been simulated (see Figure S13 of supporting information). As small differences in the simulated ozone mixing ratio have a large impact on the deactivation pathways, some deficiencies might arise in the simulation of chlorine deactivation.

4.5. Relation of Arctic Ozone Loss to Vortex Dynamics and Temperatures

In accordance with observational studies (e.g., Manney et al., 2020; Wohltmann et al., 2020), it is shown here through our CLaMS simulations that Arctic ozone depletion in 2020 was unprecedented despite the fact that halogen levels in the stratosphere have been decreasing since about the year 2000 (Engel et al., 2018; Newman et al., 2007), meaning that a decrease in chlorine-catalyzed ozone depletion would be expected. From our simulation, it is evident that in particular the low temperatures, their extension into spring, and the stable stratospheric vortex (Lawrence et al., 2020) are responsible for the strong ozone depletion observed. Wohltmann et al. (2020) indicate that the low dynamical resupply of ozone-rich air due to the strong transport barrier at the vortex edge may in addition have contributed to the observed low ozone mixing ratios. Feng et al. (2021) noted that one reason for the stable and cold vortex in this winter was an extremely weak planetary wave driving in the Northern Hemisphere indicated by an extremely low extra-tropical winter mean eddy heat flux. The increase in greenhouse gas concentrations over the last few decades has resulted in more dynamic activity and could therefore cause a less stable polar vortex (Kretschmer et al., 2018). However, the increase of greenhouse gas concentrations causes an increase in infrared radiative emissions and thus a temperature decrease in the stratosphere (e.g., Maycock et al., 2018). Rex et al. (2006) suggested that as the coldest Arctic stratospheric winters have been getting colder, this has resulted in an increasingly strong ozone loss in these winters. There is a debate about such projections based on studies using extreme value statistics (Rieder & Polvani, 2013; Rieder et al., 2014) or sunlit vortex volumes (Pommereau et al., 2013). Rieder et al. (2014) argue that the temperature decrease in the lower stratosphere is dominated by ozone depleting substances as opposed to well-mixed greenhouse gases, which dominate the temperature trend in the upper stratosphere.

As it is expected that in the upcoming decades ozone-depleting substances decline and greenhouse gases increase, the importance of dynamical processes for determining Arctic springtime ozone will likely grow (Butler et al., 2016; Portmann et al., 2012). Chemistry Climate Model (CCM) simulations show that even after 2040, when EESC has declined substantially, early springtime Arctic total column ozone in certain years can drop by about 50–100 DU below the long-term average (Bednarz et al., 2016; Langematz et al., 2014). Such losses are substantial, but are less than the loss in winter 2019/2020 reported here. Nevertheless, although stratospheric chlorine levels are decreasing, it is possible that Arctic ozone losses in the range observed in 2020 may continue to occur in the coming decades.

5. Conclusions

Arctic winter/spring 2019/2020 was exceptionally cold in the polar stratosphere and the polar vortex was stable for an unusually long period until early April, which led to significant chemical ozone depletion through the end of March and the conservation of this depleted ozone in the polar vortex until early April 2020. The extent of ozone loss has been simulated by CLaMS, where these simulations correspond well with satellite observations. Although stratospheric halogen loading (EESC) has decreased by about 11%–12% since its peak in 2000, the particular meteorological conditions in 2020 allowed enhanced levels of active chlorine to persist over a long period of time, causing unprecedented Arctic ozone depletion. Chlorine activation already started in late November 2019 and lasted until early March. Because of the low ozone values reached, a substantial production of HCl occurred in late March and April, resembling deactivation patterns seen in the Antarctic. In the vortex core average, the strongest simulated ozone depletion was 2.74 ppmv at 470 K on 30 March. The lowest simulated ozone mixing ratio in the polar lower stratosphere was about 40 ppbv. The calculated vortex core average ozone partial column depletion between the potential temperatures of 350 and 600 K was 143 DU in early April. This number is very sensitive to the representation of diabatic descent in the polar vortex. An additional ozone partial column loss of 17 DU was calculated for a simulation with enhanced descent, which might be considered as more realistic in the sense that it better fits the observed N_2O mixing ratios as a measure of diabatic descent. The partial ozone column loss

in the lower stratosphere of the reference simulation exceeds that in the simulations for the Arctic winters in 2016 (126 DU) and 2011 (106 DU), which showed the strongest ozone depletion before 2020. However, Arctic ozone depletion values in 2020 still remained below the typical values of Antarctic ozone depletion. If Arctic winters with such low temperatures and with an extension of low temperatures into spring recur in the coming decades, similarly strong springtime ozone depletion can be expected despite decreasing stratospheric chlorine loading.

Data Availability Statement

The satellite data used in this study are publicly available. MLS level 2 data (version 4) were obtained from https://acdisc.gesdisc.eosdisc.nasa.gov/data/Aura_MLS_Level2, OMI level 3 data from https://ozonewatch.gsfc.nasa.gov/data/omi and ACE-FTS data (version 3.6) from https://databace.scisat.ca/level2/ace_v3.5_v3.6. Ozone sonde data are available from the World Ozone and Ultraviolet Radiation Data Centre (WOUDC) at https://woudc.org and the Network for the Detection of Atmospheric Composition Change (NDACC) at https://www.ndacc.org. CLaMS model results in the equivalent latitude/potential temperature averages are available from https://datapub.fz-juelich.de/slcs/clams/ozoneloss_2020 (https://doi.org/10.26165/JUELICH-DATA/KET287).

Acknowledgments
The authors would like to thank the Earth System Modeling (ESM) project for funding this work by providing computing time on the ESM partition of the JUWELS supercomputer as well as the VSR commission for funding this work under the project JICG11 on the JURECA supercomputer—both systems located at the Jülich Supercomputing Centre (JSC). We would also like to thank the European Centre for Medium-Range Weather Forecasts (ECMWF) for providing the operational analyses. This paper is based on the model CLaMS which has been developed and maintained by a comprehensive team with significant programming support from Nicole Thomas. We also thank Gloria Manney, Michelle Santee and the MLS team, Peter Bernath, Kaley Walker and the ACE-FTS team as well as the OMI team for their enormous work in providing high-quality data sets. We would particularly like to thank Peter von der Gathen for providing the ozone sonde data from the Ny Ålesund station. We also thank Andreas Engel for providing the tracer correlations for Cl_y and Br_y. We are especially grateful for the constructive comments provided by three reviewers. Open access funding enabled and organized by Projekt DEAL.

References

Adams, C., Strong, K., Zhao, X., Bassford, M. R., Chipperfield, M. P., Daffer, W., et al. (2012). Severe 2011 ozone depletion assessed with 11 years of ozone, NO_2, and OClO measurements at 80 degrees N. *Geophysical Research Letters*, *39*. https://doi.org/10.1029/2011GL050478

Arnone, E., Castelli, E., Papandrea, E., Carlotti, M., & Dinelli, B. M. (2012). Extreme ozone depletion in the 2010–2011 arctic winter stratosphere as observed by MIPAS/ENVISAT using a 2-d tomographic approach. *Atmospheric Chemistry and Physics*, *12*, 9149–9165. https://doi.org/10.5194/acp-12-9149-2012

Bednarz, E. M., Maycock, A. C., Abraham, N. L., Braesicke, P., Dessens, O., & Pyle, J. A. (2016). Future Arctic ozone recovery: The importance of chemistry and dynamics. *Atmospheric Chemistry and Physics*, *16*, 12159–12176. https://doi.org/10.5194/acp-16-12159-2016

Bernath, P. F., McElroy, C. T., Abrams, M. C., Boone, C. D., Butler, M., Camy-Peyret, C., et al. (2005). Atmospheric Chemistry Experiment (ACE) Mission overview. *Geophysical Research Letters*, *32*(15). https://doi.org/10.1029/2005GL022386

Bernhard, G. H., Fioletov, V. E., Grooß, J.-U., Ialongo, I., Johnsen, B., Lakkala, K., et al. (2020). Record-breaking increases in Arctic solar ultraviolet radiation caused by exceptionally large ozone depletion in 2020. *Geophysical Research Letters*, *47*(24), e2020GL090844. https://doi.org/10.1029/2020GL090844

Boone, C. D., Walker, K. A., & Bernath, P. F. (2013). Version 3 retrievals for the Atmospheric Chemistry Experiment Fourier Transform Spectrometer (ACE-FTS). In The Atmospheric Chemistry Experiment ACE at 10: A solar occultation anthology. A. Deepak Publishing.

Burkholder, J. B., Sander, S. P., Abbatt, J. P. D., Barker, J. R., Huie, R. E., Kolb, C. E., et al. (2015). *Chemical kinetics and photochemical data for use in atmospheric studies, evaluation number 18*. (JPL Publication 15-10).

Butchart, N., & Remsberg, E. E. (1986). The area of the stratospheric polar vortex as a diagnostic for tracer transport on an isentropic surface. *Journal of the Atmospheric Sciences*, *43*(13), 1319–1339. https://doi.org/10.1175/1520-0469(1986)043<1319:taotsp>2.0.co;2

Butler, A. H., Daniel, J. S., Portmann, R. W., Ravishankara, A. R., Young, P. J., Fahey, D. W., & Rosenlof, K. H. (2016). Diverse policy implications for future ozone and surface UV in a changing climate. *Environmental Research Letters*, *11*(6). https://doi.org/10.1088/1748-9326/11/6/064017

Crutzen, P. J., Müller, R., Brühl, C., & Peter, T. (1992). On the potential importance of the gas phase reaction $CH_3O_2 + ClO \rightarrow ClOO + CH_3O$ and the heterogeneous reaction $HOCl + HCl \rightarrow H_2O + Cl_2$ in "ozone hole" chemistry. *Geophysical Research Letters*, *19*(11), 1113–1116. https://doi.org/10.1029/92GL01172

Dameris, M., Loyola, D. G., Nützel, M., Coldewey-Egbers, M., Lerot, C., Romahn, F., & van Roozendael, M. (2021). Record low ozone values over the arctic in boreal spring 2020. *Atmospheric Chemistry and Physics*, *21*(2), 617–633. https://doi.org/10.5194/acp-21-617-2021

Douglass, A. R., & Kawa, S. R. (1999). Contrast between 1992 and 1997 high-latitude spring Halogen Occultation Experiment observations of lower stratospheric HCl. *Journal of Geophysical Research*, *104*, 18739–18754. https://doi.org/10.1029/1999JD900281

Douglass, A. R., Schoeberl, M. R., Stolarski, R. S., Waters, J. W., Russell, J. M., III, Roche, A. E., & Massie, S. T. (1995). Interhemispheric differences in springtime production of HCl and $ClONO_2$ in the polar vortices. *Journal of Geophysical Research*, *100*, 13967–13978. https://doi.org/10.1029/95JD00698

Drdla, K., & Müller, R. (2012). Temperature thresholds for chlorine activation and ozone loss in the polar stratosphere. *Annales Geophysicae*, *30*, 1055–1073. https://doi.org/10.5194/angeo-30-1055-2012

Engel, A., Bönisch, H., Ostermöller, J., Chipperfield, M. P., Dhomse, S., & Jöckel, P. (2018). A refined method for calculating equivalent effective stratospheric chlorine. *Atmospheric Chemistry and Physics*, *18*(2), 601–619. https://doi.org/10.5194/acp-18-601-2018

Fahey, D. W., Gao, R. S., Carslaw, K. S., Kettleborough, J., Popp, P. J., Northway, M. J., et al. (2001). The detection of large HNO_3-containing particles in the winter Arctic stratosphere. *Science*, *291*, 1026–1031. https://doi.org/10.1126/science.1057265

Farman, J. C., Gardiner, B. G., & Shanklin, J. D. (1985). Large losses of total ozone in Antarctica reveal seasonal ClO_x/NO_x interaction. *Nature*, *315*, 207–210. https://doi.org/10.1038/315207a0

Feng, W., Dhomse, S. S., Arosio, C., Weber, M., Burrows, J. P., Santee, M. L., & Chipperfield, M. P. (2021). Arctic Ozone Depletion in 2019/20: Roles of chemistry, dynamics and the Montreal protocol. *Geophysical Research Letters*, *48*(4). https://doi.org/10.1029/2020GL091911

Garcia, R. R., & Solomon, S. (1985). The effect of breaking gravity waves on the dynamics and chemical composition of the mesosphere and lower thermosphere. *Journal of Geophysical Research*, *90*, 3850–3868. https://doi.org/10.1029/jd090id02p03850

Grooß, J.-U. (1996). *Modeling of stratospheric chemistry based on HALOE/UARS satellite data* (PhD Thesis). University of Mainz.

Grooß, J.-U., Brautzsch, K., Pommrich, R., Solomon, S., & Müller, R. (2011). Stratospheric ozone chemistry in the Antarctic: What controls the lowest values that can be reached and their recovery? *Atmospheric Chemistry and Physics*, *11*, 12217–12226. https://doi.org/10.5194/acp-11-12217-2011

Grooß, J.-U., Engel, I., Borrmann, S., Frey, W., Günther, G., Hoyle, C. R., & Müller, R. (2014). Nitric acid trihydrate nucleation and denitrification in the Arctic stratosphere. *Atmospheric Chemistry and Physics*, *14*(2), 1055–1073. https://doi.org/10.5194/acp-14-1055-2014

Grooß, J.-U., Konopka, P., & Müller, R. (2005). Ozone chemistry during the 2002 Antarctic vortex split. *Journal of the Atmospheric Sciences*, *62*(3), 860–870. https://doi.org/10.1175/jas-3330.1

Grooß, J.-U., Müller, R., Spang, R., Tritscher, I., Wegner, T., Chipperfield, M. P., et al. (2018). On the discrepancy of HCl processing in the core of the wintertime polar vortices. *Atmospheric Chemistry and Physics*, *18*, 8647–8666. https://doi.org/10.5194/acp-18-8647-2018

Grooß, J.-U., Pierce, R. B., Crutzen, P. J., Grose, W. L., & Russell, J. M., III. (1997). Re-formation of chlorine reservoirs in southern hemisphere polar spring. *Journal of Geophysical Research*, *102*, 13141–13152. https://doi.org/10.1029/96JD03505

Grooß, J.-U., & Russell, J. M. (2005). Technical note: A stratospheric climatology for O_3, H_2O, CH_4, NO_x, HCl, and HF derived from HALOE measurements. *Atmospheric Chemistry and Physics*, *5*, 2797–2807. https://doi.org/10.5194/acp-5-2797-2005

Hoppe, C. M., Hoffmann, L., Konopka, P., Grooß, J.-U., Ploeger, F., Günther, G., et al. (2014). The implementation of the CLaMS Lagrangian transport core into the chemistry climate model EMAC 2.40.1: Application on age of air and transport of long-lived trace species. *Geoscientific Model Development*, *7*(6), 2639–2651. https://doi.org/10.5194/gmd-7-2639-2014

Isaksen, I. S. A., Zerefos, C., Wang, W. C., Balis, D., Eleftheratos, K., Rognerud, B., et al. (2012). Attribution of the Arctic ozone column deficit in March 2011. *Geophysical Research Letters*, *39*, 557–560. https://doi.org/10.1029/2012GL053876

Johansson, S., Santee, M. L., Grooß, J.-U., Höpfner, M., Braun, M., Friedl-Vallon, F., et al. (2019). Unusual chlorine partitioning in the 2015/16 Arctic winter lowermost stratosphere: Observations and simulations. *Atmospheric Chemistry and Physics*, *19*, 8311–8338. https://doi.org/10.5194/acp-19-8311-2019

Jones, A. E., & Shanklin, J. D. (1995). Continued decline of total ozone over Halley, Antarctica, since 1985. *Nature*, *376*, 409–411. https://doi.org/10.1038/376409a0

Konopka, P., Steinhorst, H.-M., Grooß, J.-U., Günther, G., Müller, R., Elkins, J. W., et al. (2004). Mixing and ozone loss in the 1999-2000 Arctic vortex: Simulations with the 3-dimensional Chemical Lagrangian Model of the Stratosphere (CLaMS). *Journal of Geophysical Research*, *109*. https://doi.org/10.1029/2003JD003792

Kretschmer, M., Coumou, D., Agel, L., Barlow, M., Tziperman, E., & Cohen, J. (2018). More-persistent weak stratospheric polar vortex states linked to cold extremes. *Bulletin of the American Meteorological Society*, *99*(1), 49–60. https://doi.org/10.1175/BAMS-D-16-0259.1

Kuttippurath, J., Godin-Beekmann, S., Lefèvre, F., Nikulin, G., Santee, M. L., & Froidevaux, L. (2012). Record-breaking ozone loss in the arctic winter 2010/2011: Comparison with 1996/1997. *Atmospheric Chemistry and Physics*, *12*, 7073–7085. https://doi.org/10.5194/acp-12-7073-2012

Langematz, U., Meul, S., Grunow, K., Romanowsky, E., Oberländer, S., Abalichin, J., & Kubin, A. (2014). Future arctic temperature and ozone: The role of stratospheric composition changes. *Journal of Geophysical Research*, *119*(5), 2092–2112. https://doi.org/10.1002/2013JD021100

Lary, D. J., Chipperfield, M. P., Pyle, J. A., Norton, W. A., & Riishøjgaard, L. P. (1995). Three-dimensional tracer initialization and general diagnostics using equivalent PV latitude-potential-temperature coordinates. *Quarterly Journal of the Royal Meteorological Society*, *121*, 187–210. https://doi.org/10.1002/qj.49712152109

Lawrence, Z., Perlwitz, J., Butler, A. H., Manney, G. L., Newman, P. A., Lee, S. H., & Nash, E. R. (2020). The remarkably strong Arctic stratospheric polar vortex of winter 2020: Links to record-breaking Arctic oscillation and ozone loss. *Journal of Geophysical Research*, *125*. https://doi.org/10.1029/2020JD033271

Levelt, P. F., Oord, Van den, G. H. J., Dobber, M. R., Malkki, A., Visser, H., de Vries, J., et al. (2006). The Ozone Monitoring Instrument. *IEEE Transactions on Geoscience and Remote Sensing*, *44*(5), 1093–1101. https://doi.org/10.1109/TGRS.2006.872333

Livesey, N. J., Read, W. G., Wagner, P. A., Froidevaux, L., Lambert, A., Manney, G. L., et al. (2020). *Version 4.2x level 2 and 3 data quality and description document* (JPL D-33509 Rev. E.). Retrieved from https://mls.jpl.nasa.gov/data/v4-2_data_quality_document.pdf

Manney, G. L., & Lawrence, Z. D. (2016). The major stratospheric final warming in 2016: Dispersal of vortex air and termination of Arctic chemical ozone loss. *Atmospheric Chemistry and Physics*, *16*, 15371–15396. https://doi.org/10.5194/acp-16-15371-2016

Manney, G. L., Lawrence, Z. D., Santee, M. L., Livesey, N. J., Lambert, A., & Pitts, M. C. (2015). Polar processing in a split vortex: Arctic ozone loss in early winter 2012/2013. *Atmospheric Chemistry and Physics*, *15*(10), 5381–5403. https://doi.org/10.5194/acp-15-5381-2015

Manney, G. L., Livesey, N. J., Santee, M. L., Froidevaux, L., Lambert, A., Lawrence, Z., et al. (2020). Record-low Arctic stratospheric ozone in 2020: MLS observations of chemical processes and comparisons with previous extreme winters. *Geophysical Research Letters*, *47*(16). https://doi.org/10.1029/2020GL089063

Manney, G. L., Santee, M. L., Rex, M., Livesey, N. J., Pitts, M. C., Veefkind, P., & Zinoviev, N. S. (2011). Unprecedented Arctic ozone loss in 2011. *Nature*, *478*, 469–475. https://doi.org/10.1038/nature10556

Maycock, A. C., Randel, W. J., Steiner, A. K., Karpechko, A. Y., Christy, J., Saunders, R., et al. (2018). Revisiting the mystery of recent stratospheric temperature trends. *Geophysical Research Letters*, *45*(18), 9919–9933. https://doi.org/10.1029/2018GL078035

McKenna, D. S., Grooß, J.-U., Günther, G., Konopka, P., Müller, R., Carver, G., & Sasano, Y. (2002). A new Chemical Lagrangian Model of the Stratosphere (CLaMS): 2. Formulation of chemistry scheme and initialization. *Journal of Geophysical Research*, *107*(D15), 4256. https://doi.org/10.1029/2000JD000113

McPeters, R., Kroon, M., Labow, G., Brinksma, E., Balis, D., Petropavlovskikh, I., et al. (2008). Validation of the Aura Ozone Monitoring Instrument total column ozone product. *Journal of Geophysical Research*, *113*. https://doi.org/10.1029/2007JD008802

Morcrette, J.-J. (1991). Radiation and cloud radiative properties in the European Centre for Medium-Range Weather Forecasts forecasting system. *Journal of Geophysical Research*, *96*(D5), 9121–9132. https://doi.org/10.1029/89JD01597

Müller, R., Grooß, J.-U., McKenna, D. S., Crutzen, P. J., Brühl, C., Russell, J. M., et al. (1997). HALOE observations of the vertical structure of chemical ozone depletion in the Arctic vortex during winter and early spring 1996-1997. *Geophysical Research Letters*, *24*, 2717–2720. https://doi.org/10.1029/97GL52834

Müller, R., Grooß, J.-U., Zafar, A. M., Robrecht, S., & Lehmann, R. (2018). The maintenance of elevated active chlorine levels in the Antarctic lower stratosphere through HCl null cycles. *Atmospheric Chemistry and Physics*, *18*(4), 2985–2997. https://doi.org/10.5194/acp-18-2985-2018

Müller, R., Peter, T., Crutzen, P. J., Oelhaf, H., Adrian, G. P., Clarmann, A., et al. (1994). Chlorine chemistry and the potential for ozone depletion in the Arctic stratosphere in the winter of 1991/92. *Geophysical Research Letters*, *21*, 1427–1430. https://doi.org/10.1029/94GL00465

Nash, E. R., Newman, P. A., Rosenfield, J. E., & Schoeberl, M. R. (1996). An objective determination of the polar vortex using Ertel's potential vorticity. *Journal of Geophysical Research*, *101*, 9471–9478. https://doi.org/10.1029/96JD00066

Newman, P. A., Daniel, J. S., Waugh, D. W., & Nash, E. R. (2007). A new formulation of equivalent effective stratospheric chlorine (EESC). *Atmospheric Chemistry and Physics*, *7*(17), 4537–4552. https://doi.org/10.5194/acp-7-4537-2007

Newman, P. A., Gleason, F., McPeters, R., & Stolarski, R. (1997). Anomalously low ozone over the Arctic. *Geophysical Research Letters*, *24*, 2689–2692. https://doi.org/10.1029/97GL5238110.1029/97gl52831

Pommereau, J.-P., Goutail, F., Lefèvre, F., Pazmino, A., Adams, C., Dorokhov, V., et al. (2013). Why unprecedented ozone loss in the Arctic in 2011? Is it related to climate change? *Atmospheric Chemistry and Physics*, *13*(10), 5299–5308. https://doi.org/10.5194/acp-13-5299-2013

Pommrich, R., Müller, R., Grooß, J.-U., Konopka, P., Ploeger, F., Vogel, B., et al. (2014). Tropical troposphere to stratosphere transport of carbon monoxide and long-lived trace species in the Chemical Lagrangian Model of the Stratosphere (CLaMS). *Geoscientific Model Development*, *7*(6), 2895–2916. https://doi.org/10.5194/gmd-7-2895-2014

Portmann, R. W., Daniel, J. S., & Ravishankara, A. R. (2012). Stratospheric ozone depletion due to nitrous oxide: Influences of other gases. *Philosophical Transactions of the Royal Society B*, *367*(1593), 1256–1264. https://doi.org/10.1098/rstb.2011.0377

Portmann, R. W., Solomon, S., Garcia, R. R., Thomason, L. W., Poole, L. R., & McCormick, M. P. (1996). Role of aerosol variations in anthropogenic ozone depletion in the polar regions. *Journal of Geophysical Research*, *101*, 22991–23006. https://doi.org/10.1029/96jd02608

Rex, M., Salawitch, R. J., Deckelmann, H., Gathen, von der, P., Harris, N. R. P., Chipperfield, M. P., et al. (2006). Arctic winter 2005: Implications for stratospheric ozone loss and climate change. *Geophysical Research Letters*, *33*. https://doi.org/10.1029/2006GL026731

Rieder, H. E., & Polvani, L. M. (2013). Are recent Arctic ozone losses caused by increasing greenhouse gases? *Geophysical Research Letters*, *40*(16), 4437–4441. https://doi.org/10.1002/grl.50835

Rieder, H. E., Polvani, L. M., & Solomon, S. (2014). Distinguishing the impacts of ozone-depleting substances and well-mixed greenhouse gases on Arctic stratospheric ozone and temperature trends. *Geophysical Research Letters*, *41*(7), 2652–2660. https://doi.org/10.1002/2014GL059367

Santee, M. L., MacKenzie, I. A., Manney, G. L., Chipperfield, M. P., Bernath, P. F., Walker, K. A., et al. (2008). A study of stratospheric chlorine partitioning based on new satellite measurements and modeling. *Journal of Geophysical Research*, *113*. https://doi.org/10.1029/2007JD009057

Sheese, P. E., Walker, K. A., Boone, C. D., Bernath, P. F., Froidevaux, L., Funke, B., et al. (2017). ACE-FTS ozone, water vapor, nitrous oxide, nitric acid, and carbon monoxide profile comparisons with MIPAS and MLS. *Journal of Quantitative Spectroscopy & Radiative Transfer*, *186*, 63–80. https://doi.org/10.1016/j.jqsrt.2016.06.026

Sinnhuber, B.-M., Stiller, G., Ruhnke, R., Clarmann, von, T., Kellmann, S., & Aschman, J. (2011). Arctic winter 2010/2011 at the brink of an ozone hole. *Geophysical Research Letters*, *38*. https://doi.org/10.1029/2011GL049784

Smit, H. G. J., Straeter, W., Johnson, B. J., Oltmans, S. J., Davies, J., Tarasick, D. W., et al. (2007). Assessment of the performance of ECC-ozonesondes under quasi-flight conditions in the environmental simulation chamber: Insights from the Juelich Ozone Sonde Intercomparison Experiment (JOSIE). *Journal of Geophysical Research*, *112*. https://doi.org/10.1029/2006jd007308

Solomon, S. (1999). Stratospheric ozone depletion: A review of concepts and history. *Reviews of Geophysics*, *37*(3), 275–316. https://doi.org/10.1029/1999RG900008

Solomon, S., Portmann, R. W., Sasaki, T., Hofmann, D. J., & Thompson, D. W. J. (2005). Four decades of ozonesonde measurements over Antarctica. *Journal of Geophysical Research*, *110*(D21). https://doi.org/10.1029/2005JD005917

Strahan, S. E., Douglass, A. R., Newman, P. A., & Steenrod, S. D. (2014). Inorganic chlorine variability in the Antarctic vortex and implications for ozone recovery. *Journal of Geophysical Research*, *119*. https://doi.org/10.1002/2014JD022295

Tilmes, S., Müller, R., Grooß, J.-U., & Russell, J. M. (2004). Ozone loss and chlorine activation in the Arctic winters 1991–2003 derived with the tracer-tracer correlations. *Atmospheric Chemistry and Physics*, *4*(8), 2181–2213. https://doi.org/10.5194/acp-4-2181-2004

Tritscher, I., Grooß, J.-U., Spang, R., Pitts, M. P., Poole, L. R., Müller, R., & Riese, M. (2019). Lagrangian simulation of ice particles and resulting dehydration in the polar winter stratosphere. *Atmospheric Chemistry and Physics*, *19*, 543–563. https://doi.org/10.5194/acp-19-543-2019

Tritscher, I., Pitts, M. C., Poole, L. R., Alexander, S. P., Cairo, F., Chipperfield, M. P., et al. (2021). Polar stratospheric clouds: Satellite observations, processes, and role in ozone depletion. *Reviews of Geophysics*. *59*(2), e2020RG000702. https://doi.org/10.1029/2020RG000702

Voigt, C., Schlager, H., Luo, B., Dörnbrack, A., Roiger, A., Stock, P., et al. (2005). Nitric acid trihydrate (NAT) formation at low NAT supersaturation in polar stratospheric clouds (PSCs). *Atmospheric Chemistry and Physics*, *5*, 1371–1380. https://doi.org/10.5194/acp-5-1371-2005

Ward, S. M., Deshler, T., & Hertzog, A. (2014). Quasi-Lagrangian measurements of nitric acid trihydrate formation over Antarctica. *Journal of Geophysical Research*, *119*, 245–258. https://doi.org/10.1002/2013JD020326

Weber, M., Dikty, S., Burrows, J., Garny, H., Dameris, A., Abalichin, J., et al. (2011). The Brewer-Dobson circulation and total ozone from seasonal to decadal time scales. *Atmospheric Chemistry and Physics*, *11*(21), 11221–11235. https://doi.org/10.5194/acp-11-11221-2011

Wegner, T., Grooß, J.-U., Hobe, von, M., Stroh, F., Sumińska-Ebersoldt, O., Volk, C. M., & Müller, R. (2012). Heterogeneous chlorine activation on stratospheric aerosols and clouds in the arctic polar vortex. *Atmospheric Chemistry and Physics*, *12*, 11095–11106. https://doi.org/10.5194/acp-12-11095-2012

Wegner, T., Pitts, M. C., Poole, L. R., Tritscher, I., Grooß, J.-U., & Nakajima, H. (2016). Vortex-wide chlorine activation by a mesoscale PSC event in the Arctic winter of 2009/10. *Atmospheric Chemistry and Physics*, *16*, 4569–4577. https://doi.org/10.5194/acp-16-4569-2016

Wilmouth, D. M., Stimpfle, R. M., Anderson, J. G., Elkins, J. W., Hurst, D. F., Salawitch, R. J., & Lait, L. R. (2006). Evolution of inorganic chlorine partitioning in the Arctic polar vortex. *Journal of Geophysical Research*, *111*. https://doi.org/10.1029/2005JD006951

WMO. (2018). *Scientific assessment of ozone depletion: 2018*. Global Ozone Research and Monitoring Project–Report No. 58.

Wohltmann, I., Gathen, von der, P., Lehmann, R., Maturilli, M., Deckelmann, H., Manney, G. L., et al. (2020). Near complete local reduction of Arctic stratospheric ozone by severe chemical loss in spring 2020. *Geophysical Research Letters*, *47*. https://doi.org/10.1029/2020GL089547

Zhong, W., & Haigh, J. D. (1995). Improved broadband emissivity parameterization for water vapor cooling rate calculations. *Journal of the Atmospheric Sciences*, *52*(1), 124–138. https://doi.org/10.1175/1520-0469(1995)052⟨0124:IBEPFW⟩2.0.CO;2